Mid-level visual features engage V4 to support sparse object recognition under uncertainty

Leyla Loued-Khenissi[1], Elsa Scialom[2], Antoine Lutti[1] , Michael Herzog[2], Bogdan Draganski[1, 3,4]

[1] Laboratory for research in Neuroimaging – LREN, Département des Neurosciences Cliniques, Lausanne University Hospital, Lausanne, Switzerland
[2] Laboratory of Psychophysics, BMI, Ecole Polytechnique de Lausanne (EPFL), Lausanne, Switzerland
[3]Department of Neurology, Inselspital, Bern University Hospital, University of Bern, Bern, Switzerland
[4]University Institute for Diagnostic and Interventional Neuroradiology, Bern University Hospital, University of Bern, Bern, Switzerland

Running title: V4 for Object Recognition

Keywords: Object recognition; V4; fMRI; cortical prosthesis

Corresponding author: Leyla Loued-Khenissi lkhenissi@gmail.com; ORCID: 0000-0003-3241-6492

Abstract

Cortical visual prostheses have long promised to restore sight by directly stimulating the visual cortex, but current approaches remain limited. Conventional V1-targeted implants evoke isolated phosphenes that rarely support coherent object recognition, largely due to the sparse electrode arrays feasible for implantation. Here we examined whether mid-level features, specifically curve segments associated with area V4, provide a more efficient substrate for artificial vision. Using fMRI, 24 participants performed an object recognition task with stimuli fragmented into either phosphene-like dots or curve segments at graded densities. Behaviorally, curve segments enabled recognition at lower density thresholds than phosphenes, yielding steeper psychometric slopes and higher accuracy. Neuroimaging revealed that while both fragment types engaged V1, only curve segments recruited V4, and correct recognition of segments relative to phosphenes elicited widespread responses across temporal, parietal, and insular cortices. Mediation analyses further showed that recognition from phosphenes relied on anterior cingulate cortex (ACC) involvement with higher stimulus uncertainty, whereas segment-based recognition depended primarily on visual cortex. Together, these results demonstrate that mid-level feature fragments confer both perceptual and neural advantages over phosphenes, reducing reliance on downstream uncertainty resolution. V4 thus emerges as a promising target for next-generation cortical prostheses, offering a path toward sparser yet more informative stimulation strategies.

Introduction

Vision is one of the most important human faculties, yet approximately 40 million people worldwide suffer from severe visual impairments or blindness that significantly reduce quality of life. Retinal prostheses have shown partial success in specific degenerative conditions, but their performance is constrained by the dependence on residual retinal circuitry and coarse resolution (Erickson-Davis & Korzybska, 2021). This has motivated a long-standing interest in cortical visual prostheses, which bypass the eye to stimulate visual cortex directly. Electrical stimulation of the occipital lobe has been known for over a century to induce phosphenes — points of light perceived in the absence of external input — confirming the basic plausibility of such an approach (S. C. Chen et al., 2009).

Despite this conceptual promise and ongoing clinical trials (Fernández et al., 2021), no safe and reliable cortical prosthesis has been realized to date. Current devices face numerous technical and biological challenges (Borda & Ghezzi, 2022). Compared with cochlear implants, which act on an accessible single nerve, cortical devices require invasive neurosurgery and must operate with relatively few stable electrodes (Liu et al., 2022). Targeting V1 has been the default strategy because stimulation at this site reliably produces phosphenes. However, because each electrode produces a unique point of light, reconstructing coherent shapes requires a prohibitively high electrode density . In macaque studies, small-scale intracortical stimulation in V1 evoked stable, spatially specific percepts over years (Davis et al., 2012), whereas higher-density Utah array implants show reliable initial performance but rapid degradation of signal quality and perceptual stability over months (Chen et al., 2020), highlighting a trade-off between channel count and long-term functional reliability in cortical visual prostheses. In humans, multi-electrode stimulation of early visual areas produces spatially organized but unstable percepts: simultaneous stimulation in V1–V3 evokes multiple phosphenes that rarely merge into coherent forms (Bosking et al., 2022) and perceptual quality varies widely with training, fixation, and electrode mapping (Oswalt et al., 2021). Together, these results indicate that while direct cortical stimulation can elicit basic visual sensations, a “connect-the-dots” approach yields unstable, fragmentary percepts rather than meaningful vision (Sanchez-Garcia et al., 2018).

An important next step is to determine how mid-level visual organization can be leveraged to transform fragmented inputs into coherent percepts. One possible solution is to move beyond V1 and target downstream areas that encode mid-level visual features. Area V4 is an

especially promising candidate: it is tuned to curved segments and intermediate shape features (Carlson et al., 2011; Wei et al., 2018), and contributes directly to object recognition (Roe et al., 2012). Human neuroimaging and retinotopic mapping confirm that V4 contains curvature-selective domains and occupies a pivotal position along the ventral visual pathway (Winawer & Witthoft, 2015). Psychophysical and fMRI evidence further shows that contour integration and curvature processing emerge through V4 and strengthen toward lateral occipital cortex, linking mid-level structure to global shape perception (Kuai et al., 2017; Lawrence et al., 2023). These findings align with classic recognition-by-components theory that emphasizes curvature and collinearity as litmus tests for object recognition (Biederman, 1987). Representations at this stage may provide a more efficient basis for percept formation than discrete point-like inputs, even without direct stimulation.

There have been very limited studies investigating V4 stimulation's effect on vision. Shiozaki and colleagues (Shiozaki et al., 2012) showed that microstimulation of disparity-selective clusters in macaque V4 biases depth judgments, establishing a causal role for V4 neurons in depth discrimination. Another study in macaques found V4 microstimulation had virtually no effect on visual stimulus detection thresholds (Dagnino et al., 2015) but a more recent study found microstimulation of area V4 in macaques led to improved performance in a visual detection task (Kienitz et al., 2022). Yet it remains unknown how V1 and V4 contribute to recognizing objects from sparse, fragmented representations composed of either low-level points or mid-level segments. Although this possibility has been raised in animal studies, it remains largely unexplored in humans. Moreover, no study has directly tested whether the perceptual benefits of contour continuity, a feature central to mid-level visual organization, can be traced to V4 processing, which may also ultimately support more coherent cortical prosthetic vision.

By integrating evidence from cortical prosthesis research and mid-level vision, we examine whether the perceptual gains afforded by contour continuity originate from mid-level curvature and grouping mechanisms in area V4, identifying a potential neural substrate for more coherent cortical prosthetic vision. Here, we addressed this question using fMRI and a task designed to simulate recognition from prosthesis-like input. Participants viewed fragmented outlines of objects composed of either phosphene-like dots or curve segments at increasing density levels, and then identified the correct object from a choice grid. This design allowed us to test three specific hypotheses. First, we hypothesized that curve

segments would facilitate more efficient recognition than phosphenes, requiring fewer fragments for successful identification (H1). Second, we hypothesized that successful recognition of curve segments would preferentially engage mid-level extrastriate cortex, specifically V4, in contrast to phosphenes, which would rely more heavily on V1 (H2). Finally, we hypothesized that correct recognition under sparse and uncertain conditions would recruit the anterior cingulate cortex (ACC) as a downstream control region, reflecting its established role in perceptual uncertainty (Levinson et al., 2021). We further predicted that this contribution would be stronger for phosphenes, which provide less reliable sensory information, than for curve segments (H3). By identifying how the brain reconstructs objects from sparse cues, this study bridges visual neuroscience and neuroengineering, offering representational principles to guide the next generation of cortical visual prostheses.

Results

Behavioral

To examine specific differences between fragments types, our main area of interest, the following results reflect only fragmented image trials.

To determine if object recognition occurs at a lower density threshold with segments rather than phosphenes, we computed individual subjects proportion of correct responses for each density level for each fragment type, and fit a logistic model to these values of the form

$$(1)\ \frac{1}{1+e^{-k*(x-PSE)}}$$

This fit provides the *k* parameter, the steepest slope of the curve, indicative of a transition between incorrect and correct; and the points of subjective equality (PSE), indicating the density level at which this transition occurs. We find, for segments, a mean of PSE = 31.74, (SD = 18.60) and for phosphenes, a mean PSE of = 43.44 (SD = 13.09). A direct comparison of these fits show a significant difference (segments < phosphenes): $t = -5.35$, $p < 0.001$ (Figure 1a).

The mixed-effects regression model assessing factors influencing accuracy shows significant positive effects of segment fragment type ($t = 4.110$, $p < 0.001$) and density ($t = 13.314$, $p < 0.001$). Accuracy is negatively associated with reaction time ($t = -4.444$, $p < 0.001$). In addition, accuracy is reduced by the interactions of segment fragment type with density (t = -

3.479, $p < 0.001$) and with entropy ($t = -2.591$, $p = 0.010$). The effect of entropy alone is nonsignificant ($t = 0.140$, $p = 0.888$), as is the interaction of segment fragment type with reaction time ($t = -0.753$, $p = 0.451$) (Figure 1b).

The mixed-effects regression model assessing factors influencing confidence ratings shows significant positive effects of accuracy ($t = 11.809$, $p < 0.001$) and density ($t = 12.901$, $p < 0.001$). Confidence is negatively associated with entropy ($t = -5.760$, $p < 0.001$). The main effect of segment fragment type is nonsignificant ($t = -0.230$, $p = 0.818$), as are the effects of confidence reaction time ($t = -0.943$, $p = 0.346$) and the interactions of segment fragment type with density ($t = 0.910$, $p = 0.363$), accuracy ($t = 0.245$, $p = 0.806$), confidence reaction time ($t = -0.921$, $p = 0.357$), and entropy ($t = 1.110$, $p = 0.267$) (Figure 1).

Figure 1: Behavioral analysis of responses. a) and b) T statistics for different predictors of accuracy and confidence. Red dashed lines indicate significance thresholds for $p = 0.05$. c) and d) Psychometric curves for phosphene and segment trials fit to a logistic function. Pink curves indicate individual subject performance in phosphene trials against fragment density levels. Blue curves indicate individual subject performance in segment trials against fragment density levels. The black curve indicates the grand mean fit.

Taken together, the hypothesis that segment fragment type and density enhance object recognition were confirmed. These hypotheses are further edified by the positive effects of accuracy and density on metacognitive confidence, which provide evidence that individuals are aware of their performance quality.

Neuroimaging - Whole brain results

Control Trials: Contour and RGB Trial Tests at Stimulus Presentation

RGB statistical maps showed no significant responses. Contour image trials yielded clusters in the bilateral inferior temporal gyri, fusiform gyri, left angular gyrus, left hippocampus and bilateral inferior frontal gyrus. Contour trials tested as positive against all fragment types showed clusters bilaterally in the fusiform gyrus (as did contour trials tested against segment trials) and clusters in the left fusiform and right inferior temporal gyrus in phosphene trials. All fragmented image trials tested as greater than contour trials yielded a widespread network of clusters in the following regions: bilateral precentral gyrus, left supplementary motor cortex, right cerebellum, left parietal operculum, left angular gyrus, left thalamus, left

putamen, left cuneus, bilateral middle frontal gyrus, left inferior occipital gyrus, left cuneus, left mid cingular gyrus, right lingual gyrus, and right postcentral and supramarginal gyri. Phosphene trials greater than contour trials showed clusters in right precentral gyrus and right inferior occipital gyrus. Segment trials greater than contour trials showed a more extensive pattern of clusters in left supramarginal and superior temporal gyri, as well as right lingual gyrus. With respect to contour trials greater than RGB, numerous clusters emerged including: bilateral inferior, middle temporal and fusiform gyri, right parahippocampal and angular gyri, and left anterior insula. No other tests on RGB trials yielded significant clusters.

Phosphene and Segment Trial Tests

Phosphene trials at cue presentation onsets yielded bilateral clusters in the middle temporal gyrus, left angular gyrus and extensively in the cingulate (Figure 2a and 2b). Segment trials yielded significant clusters in similar regions, as well as in the thalamus. Phosphene density was associated with significant bilateral responses in the fusiform gyrus, while segment density was associated with right mid and left inferior occipital cortex (Figure 2c and 2d). Phosphene confidence was associated with left inferior occipital cortex, while segment confidence showed a similar pattern of response that did not survive correction for multiple comparisons (Figure 2f)(Table 2). When testing phosphene versus segment contrasts directly, only one test yielded significant results, at response onsets: correct segment trials greater than correct phosphene trials showed significant results in the cerebellum, middle temporal lobe, bilateral supramarginal and postcentral gyri, middle and anterior cingulate, as well as the left temporal pole and left anterior insula, among other regions (Table 3). Critically, the cluster with a peak in the cerebellum extends over area V4 on the right (Figure 3b). No other tests examining phosphene versus segment trials yielded significant results.

Figure 2. Whole brain results for different fragment conditions. a) Phosphene trials at fragmented stimulus presentation trigger responses in a large clusters centered on the middle and anterior cingulate, extending to the thalamus and pallidum. b) Curve segment trials shows a similar pattern to phosphene trials, albeit with more conservative spatial extents in the same significant regions. d) and c) Contrast maps for t-tests on fragment densities in both conditions yield significant responses in the occipital cortex. e) and f) Confidence in both fragment types shows a highly similar response pattern to density levels, showing the direct relationship between the two, as seen in behavioral measures, although confidence ratings for

segment trials did not survive correction for multiple comparisons. Maps shown are thresholded at p = 0.05 FWE, cluster corrected (k = 25).

Figure 3. Whole brain results by fragment type at trial response. a) Correct curve segment trials tested against correct phosphene trials yields extensive responses in the occipital cortex encompassing area V4, as well bilateral middle temporal gyri, part of the visual ventral stream. In addition, this contrast yielded responses in the left insula, right inferior frontal gyrus and right parietal areas as well as a significant cluster in the anterior cingulate cortex. b) Statistical map of correct segments contrasted against correct phosphenes (orange) overlaid on the ROI of area V4, showing overlap (blue). c) Mediation analysis. Brain regions mediating the link between heightened uncertainty in phosphenes and correct performance include the anterior cingulate cortex (ACC).

Table 1. Contrast results at stimulus presentation onsets

Segments							
p_FWE_corr_	Cluster size k	p_FWE_corr__1	T	x	y	z	Region_AAL3v1
0	1069	0.003	8.15	-46	-74	40	Angular_L
0	6602	0.004	7.95	-6	-8	2	Thal_MDm_L
0	1499	0.025	6.83	62	-56	6	Temporal_Mid_R
0	723	0.131	5.86	0	-28	42	Cingulate_Mid_L
0.005	460	0.316	5.3	-54	-22	-14	Temporal_Mid_L
0.034	298	0.468	5.02	-14	-16	-40	Brainstem
Phosphenes							
p_FWE_corr_	Cluster size k	p_FWE_corr__1	T	x	y	z	Region_AAL3v1
0	16085	0	10.32	6	-2	-4	Accumbens, R, extending into ACC
0	2012	0	10.04	-42	-68	50	Angular_L, extending to MCC
0	2617	0.001	8.9	48	-42	2	Temporal_Mid_R
0	1716	0.034	6.8	-52	-22	-20	Temporal_Inf_L
0.013	300	0.099	6.18	-20	-48	4	Precuneus_L
0.007	342	0.133	6.01	28	-84	-32	Cerebellum_Crus1_R
0.023	265	0.191	5.78	-22	-86	-34	Cerebellum_Crus2_L
Phosphenes, Density							

p_FWE_corr_	Cluster size k	p_FWE_corr__1	T	x	y	z	Region_AAL3v1
0	2374	0.023	6.9	30	-58	-12	Fusiform_R
0	2534	0.048	6.47	-30	-60	-10	Fusiform_L
Segments, Density							
p_FWE_corr_	Cluster size k	p_FWE_corr__1	T	x	y	z	Region_AAL3v1
0	2132	0.016	6.87	36	-84	4	Occipital_Mid_R
0	1191	0.094	5.86	-22	-90	-8	Occipital_Inf_L
Phosphenes, Confidence							
p_FWE_corr_	Cluster size k	p_FWE_corr__1	T	x	y	z	Region_AAL3v1
0	5390	0.03	6.79	-38	-82	-10	Occipital_Inf_L

Table 2. Contrast results at response onsets

Segment Correct > Phosphene Correct							
p_FWE	k	p_FWE	T	x	y	z	Region_AAL3v1
0	844	0.016	7.17	-50	12	-14	Temporal_Pole_Sup_L
0	1903	0.044	6.6	30	-60	-20	Cerebellum_6_R
0	2343	0.098	6.12	56	-42	32	SupraMarginal_R
0	2731	0.126	5.97	-44	-34	32	SupraMarginal_L
0.003	436	0.14	5.91	-50	-30	0	Temporal_Mid_L
0.001	533	0.198	5.7	50	-34	-4	Temporal_Mid_R
0.001	536	0.372	5.28	-6	-26	40	Cingulate_Mid_L

ROI Analysis

To explicitly test our hypotheses regarding specific visual areas preferentially relating to specific fragment types, we examined those whole brain contrasts relating to different fragment trials that yielded significant responses using an ROI approach. Specifically, we tested contrast images on correct phosphene trials versus correct segment trials at response onset; phosphene trials alone, at stimulus onset; and segment trials alone, at stimulus onset. The *a priori* ROIs selected included: V1 (bilateral, ventral and dorsal); V4 (bilateral); and lateral occipital cortex (2 regions, bilateral). The first two regions are of direct interest to our hypothesis and the LOC was added as a region known to be implicated in object recognition. The specific ROIs used were taken from a probabilitic retinotopic atlas (L. Wang et al.,

2015). Of the contrasts tested, we found that phosphene trials at stimulus presentation elicited significant responses in the right lateral occipital cortex (1 and 2) and bilaterally in V1 (ventral). Segment trials yielded no significant responses in any of the ROIs tested. Correct segment trials greater than correct phosphene trials however yielded significant responses in bilateral V1 (ventral) and V4 (Table 3).

Table 3. Mediation analysis on regions implicated in the relationship between stimulus uncertainty and accuracy

Peak	peak			
p(FWE-corr)	T	x	y	z
Phosphenes, stimulus presentation onset				
roi14_R, lateral occipital cortex 2				
0.034	4.53	50	-74	28
roi15_R, lateral occipital cortex 1				
0.048	4.43	54	-70	20
roi1_R, V1 ventral				
0.020	4.91	48	-44	-14
Phosphene Correct < Segment Correct, response onset				
roi1_L, V1 ventral				
0.023	4.9	-6	-72	-10
roi1_R, V1 ventral				
0.009	5.36	12	-76	-12
roi7_L, hV4				
0.021	4.78	-8	-80	-16
roi7_R, hV4				
0.002	5.94	14	-68	-10

Mediation Analysis

We next sought to identify brain areas involved in mediating the relationship between stimulus uncertainty, computed above, and correct object recognition for each fragment type. We found that correct responses in phosphene fragments under higher uncertainty were dependent on the anterior cingulate cortex (Figure 3c) and areas V1 and V4, while in segments, relied only on V4.

Table 5. Results of mediation effect between uncertainty in visual stimulus and accuracy

Phosphenes, mediation *ab* effect					
Name	x	y	z	voxels	maxstat
V1	0	-78	-8	4	7.1
ACC	2	26	-6	26	9.97
V1	2	-100	4	1	5.91
V1	-8	-104	8	2	8.96
V1	-2	-102	8	1	20.76
V4	32	-94	12	6	8.01
Segments, mediation *ab* effect					
Name	x	y	z	voxels	maxstat
V4	14	-68	-6	3	7.19

Discussion

In this study, we queried three hypotheses relating to object recognition from sparse visual information. We asked 1) whether curve segments provide a more efficient basis for object recognition than low-level phosphenes; 2) if recognition from these different fragment types would recruit distinct visual areas, with V4 supporting segments and V1 supporting phosphenes; and 3) that successful recognition under uncertainty would depend on downstream cortical circuitry. Our behavioral results confirmed the first hypothesis: segments required lower fragment densities than phosphenes and yielded higher accuracy and confidence as fragment density increased. In line with the second hypothesis, only curve segments elicited significant BOLD responses in area V4, whereas phosphenes primarily engaged V1. Whole-brain contrasts showed that correct recognition of segments, relative to phosphenes, evoked a more widespread network response. To address the third hypothesis, mediation analyses was conducted to query whether correct recognition under uncertainty was supported by the ACC and visual cortex: for phosphenes, ACC (together with V1/V4) mediated successful object recognition, whereas this relationship was mediated primarily through V4 for segments, suggesting the latter reduce perceptual uncertainty and may rely more on sensory input rather than a downstream, cognitive mediation.

Implications for Visual Prosthetics & Cortical Hierarchies (H1)

Our behavioral results suggest that eliciting curve segments, rather than phosphenes, may require fewer cortical stimulations, offering an empirically grounded means by which to simplify both the design and implantation of visual prostheses for the blind. Segments enabled accurate object recognition at lower density thresholds than phosphenes, confirming our first hypothesis (H1) that mid-level visual features provide a more efficient code for object recognition. This is in line with previous work showing that adding contour information to phosphenes improved letter recognition in simulated prosthetic vision (Kiral-Kornek et al., 2014). At the neural level, we found shared V1 responses for both fragment types but a unique V4 response for segments. This finding lays the groundwork for exploratory stimulation of V4 in patients, to test whether curve segment perception can be artificially induced. Direct stimulation of ventral visual cortex in humans (Parvizi et al., 2012; Rangarajan et al., 2014) shows that perceptual outcomes depend on both cortical site and attentional state, implying that any V4-based prosthetic interface will require task- or context-dependent calibration. Previous efforts to artificially stimulate phosphenes in extrastriate areas have been successful in V2 and V3, and less promising in V5 and LOC (Schaeffner & Welchman, 2017). Studies focusing on V4 stimulation in macaques have been inconsistent with one finding no enhancement of V1 phosphene detection thresholds (Dagnino et al., 2015), and another, increased stimulus detection (Kienitz et al., 2022). Our data, in conjunction with very recent layer fMRI mapping of curvature-preference domains within human V4 (Zamboni et al., 2025), suggest this region encodes precisely the type of mid-level contour information that could be exploited by cortical stimulation to yield more coherent percepts than point-based inputs. Critically, V4 emerges as a promising alternative or complementary target to V1 for prosthetic development, offering the potential for sparser yet more informative stimulation patterns.

Beyond the visual hierarchy, our results highlight a mediating role for the anterior cingulate cortex (ACC). Both fragment types engaged the ACC at stimulus presentation, but mediation analysis showed that phosphene-based recognition relied more heavily on ACC contributions, consistent with its broader role in resolving uncertainty (Levinson et al., 2021; O'Reilly et al., 2013; Y. Wang et al., 2017) including visual uncertainty (Levinson et al., 2021). This downstream involvement may help explain why artificially induced phosphene perception is so variable across individuals: differences in the efficacy of cingulate-driven resolution may

amplify variability in conscious phosphene experience (Phylactou et al., 2023) and further echoes reports from human stimulation work showing task-dependent perceptual modulation in ventral cortex (Parvizi et al., 2012), supporting the view that prosthetic percepts will necessarily interact with cognitive state and attentional control.

Theoretical Context & Model Interpretations (H2 & H3)

These results dovetail with predictive coding accounts in which ACC provides corrective or prior-based input when sensory evidence is poor or sparse (Alexander & Brown, 2014; Gold & Stocker, 2017; Kéri et al., 2004; Rushworth & Behrens, 2008). Phosphenes, being more ambiguous, appear to demand stronger ACC contributions, while segments reduce uncertainty by engaging mid-level visual areas more directly. This interpretation is further supported by human fMRI evidence that V4 contributes to global shape integration and curvature tuning (Lawrence et al., 2023), and that contour-integration dynamics over time engage higher ventral areas beyond V1 (Kuai et al., 2017). Together with curvature-selective domains revealed in V4 (Pasupathy et al., 2020; Zamboni et al., 2025), these results converge on a mid-level mechanism by which contour continuity reduces uncertainty and stabilizes recognition(Choi et al., 2018) and further aligns with findings showing that local feedback from the extrastriate cortex to V1 is an important mechanism enabling object recognition under challenging conditions such as with fragmented, unclear or occluded objects (S. Chen et al., 2021; Wyatte et al., 2014).

A further dimension to this interpretation comes from the confidence data. Confidence judgments correlated with activity in visual cortex, suggesting that metacognitive monitoring in this task is at least partly contained within the sensory system itself (Heereman et al., 2015) though other studies have found evidence of metacognitive tracking elsewhere in the brain (Balsdon et al., 2021; Molenberghs et al., 2016). This has direct implications for prosthetics: artificial stimulation must not only reach an expected perceptual threshold but also be consciously registered in the individual. Confidence ratings offer a behavioral window onto perceptual quality, an index that could guide calibration in closed-loop prosthetic systems. If a percept is consistently accompanied by low confidence, even if objectively "seen" as confirmed by neuroimaging responses in the visual cortex, it may fail to provide functional utility (Meuwese et al., 2014; Michel et al., 2024). Future closed-loop prosthetic systems might incorporate confidence-like feedback or adaptive encoding to maintain perceptual stability across cognitive states.

Limitations & Future Directions

Our study has several limitations. While fMRI provides insight into brain mechanisms, it still falls short of causal explanations. Future work should employ causal interventions such as TMS or intracortical stimulation to confirm whether segment-like percepts can be elicited by stimulating V4. Second, the generalizability of our findings to other fragment types remains to be determined; the perceptual efficiency of segments may depend on their specific structure. Finally, although V4 stimulation offers theoretical advantages, clinical translation faces challenges including surgical access, stimulation thresholds, and the need for precise electrode targeting. These challenges parallel those faced in existing intracortical prosthesis trials, where electrode stability and mapping drift remain unresolved issues (Oswalt et al., 2021). Addressing these challenges will require integrating causal stimulation studies with computational modeling approaches capable of predicting perceptual outcomes from cortical dynamics.

Broader Relevance

These results inform the next generation of visual prostheses. Existing phosphene-based devices rely on dense V1 stimulation, yet often yield variable and unstable percepts. By showing that curve segments engage V4 and reduce the need for ACC-driven resolution, our work suggests a new avenue for prosthetic design: stimulation strategies that approximate mid-level features rather than isolated phosphenes. Moreover, our findings can enrich computational prosthetic simulators by incorporating system-level constraints such as ACC stabilization. Recent computational pipelines now enable biologically plausible, differentiable simulators that optimize stimulation parameters end-to-end (Fine & Boynton, 2024; van der Grinten et al., 2024). Incorporating behavioral priors favoring contour continuity and curvature structure into these simulators could bias optimization toward activation patterns that exploit cortical organization for perceptual coherence. Similarly, human-in-the-loop deep learning frameworks for prosthetic encoding (Granley et al., 2023) could integrate these mid-level priors to personalize stimulation patterns that minimize crowding and energy requirements. Thus the “segment advantage” identified here not only clarifies the processes supporting recognition under sparse input but also provides a computational constraint for the emerging class of virtual-patient simulators and adaptive encoders aimed at restoring functional vision.

Methods

Population

The study was conducted at the Laboratoire de Recherche en Neuroimagerie (Centre Hospitalier Universitaire Vaudois, Lausanne, Switzerland) and approved by the Commission d'éthique de la Recherche, Vaud. Participants were recruited from the general population and provided with study information two days prior to the session. On the day of testing, they reviewed and signed informed consent. Inclusion criteria were age 18–45 and good general health; exclusion criteria were self-reported psychiatric or neurological diagnoses, current or recent psychotropic medication, claustrophobia, and metal or other implants incompatible with MRI. Visual acuity was screened with the Fribourg Visual Acuity test (Landolt C); all participants met the minimum requirement of logMAR ≤ 0.3 (20/40 Snellen equivalent). After screening, the experimenter explained MRI procedures and task instructions before participants entered the scanner. Data were collected between April and May 2024.

Cohort

The study recruited 27 participants, of which 24 were retained. Three participants were excluded due to problems with the MR headcoil during acquisition. The cohort included 24 participants (11females) that completed the experiment, with 23 included in image analysis. One participant had to be excluded from imaging analysis for faulty timing recordings. As a control for performance, we verified that participants made no more than 1 error of object recognition for contour and RGB trials. All participants passed this threshold.

MRI acquisition

MRI data were acquired on a 3T Siemens Prisma scanner (Siemens, Erlangen, Germany). For each participant, functional data was acquired using a custom-made dual-echo 2D gradient-echo EPI sequence with echo times 17.4 and 35.2ms. The number of slices was 40 and the repetition time was TR = 2.48 s. The radio-frequency excitation flip angle was 90°, in-plane resolution was 3mm. Two functional scans of approximately 20 min each were acquired during task performance. B_0-field mapping data were acquired using a 2D gradient-recalled sequence (TR = 700 ms, TE = 7.38 ms, flip angle = 80°, 64 × 64 × 64 voxels, ≈ 3 mm isotropic) to correct for geometric distortions in the EPI images. T1-weighted anatomical data scan was also acquired using a 3D MPRAGE sequence with the following parameters: TR =

2000 ms, TE = 2.39 ms, flip angle = 9°; matrix = 232 × 256 × 176; voxel size ≈ 1 mm isotropic.

Stimulus generation procedure

Experimental stimuli consisted in fragmented images containing phosphenes or curved segments along object's contours. We followed the fragmentation procedure used in (Lonnqvist et al., 2025) and (Scialom et al., 2024) . The fragmentation algorithm takes an RGB image as input, extracts its contours and places phosphenes and curved segments at the same pixel coordinates along the object's starting outlines. To make both stimulus types comparable, phosphene widths were equal to segment lengths, spanning approximately 0.27 arcdeg. A density of 100% fragments corresponds to the maximum number of fragments that can outline the object's contours. The set of segments was taken from (Mineault et al., 2013)), as it triggered specific V4 activity in macaque monkeys. Details of the algorithm are described in (Scialom et al., 2024).

Task procedure

Prior to behavioral data collection and following the acquisition of the T1-MPRAGE anatomical scan, participants performed 5 practice trials of the task in the scanner. These trials employed stimuli that were not used in the experimental task. Participants were free to communicate with the experimenter via the microphone during the practice session in case of questions. Physiological measures (cardiac and respiratory) were recorded with a BioPac system. Once participants confirmed their readiness to perform the task, the first of two-trial series was launched.

In total, participants performed a total of 144 trials divided into two blocks. Stimuli were taken from the Bank of Standardized Stimuli and consisted of common objects (Brodeur et al., 2010). Eight distinct objects were selected as target stimuli and an additional 12 were selected as decoys. The 8 target stimuli were fragmented into either dot (phosphene condition) or curve segment (segment condition) outlines at the following fragment density levels: 12%, 16%, 21%, 27%, 35%, 46%, 59% and 77%, following an exponential fit previously used in (Torfs et al., 2010).

In each block, 4 distinct target objects were presented, in a randomized fashion across objects and fragment condition, at increasing fragment density levels (8), followed by the same 4 objects shown in full (white) contour on a black background; and then the same 4 target

objects shown in full RGB. Each trial began with the presentation of a black fixation cross on a grey background. Participants were asked to perform an object recognition task. At each trial, an image of an object (15 x 15 visual degrees; cue) was first briefly presented (120 ms) , followed by a black fixation cross on a grey background (6 s). Then, participants were shown a 3 * 3 grid of different objects in full color at a size of 5 * 5 degrees. This grid contained 5 decoys and 4 possible target stimuli, including one image of object category that was previously shown (Target). While the target was the same object as the cue, it was not the same image, but an example from a given image category (e.g. “boots”). For instance, the cue may have been a pair of glasses oriented towards the bottom left of the screen, and the target, oriented towards the bottom right. Participants were asked to select the previously shown object from the grid using a button response box. Following their selection, they were shown another black fixation cross on a grey background for approximately 6 s. Finally, participants were asked to provide a metacognitive confidence report on a 1-10 scale (Figure 4a).
All images were shown with white fragments on a black background, except for the RGB images, which were shown on a grey background. All code was written in Python using the PsychoPy presentation library.

Figure 1: a) Sample trial. Participants were briefly shown (120 ms) an image, composed of either white curve segments or phosphenes (dots) on a black background. The image here shows a pair of glasses at a fragment density of 21%. Participants are then shown a 3*3 grid of objects, including target stimuli as well as decoy objects and asked to navigate the grid to find the matching object. Matching objects always varied in their identity. Participants were then asked to rate their confidence in their choice. b) Retinotopic map of regions selected for ROI analysis, inluding lateral occipital cortex (LOC) and areas V1 and V4 ((L. Wang et al., 2015).

Data Analysis

Behavioral

To characterize perceptual sensitivity, individual psychometric curves were fit separately for phosphenes and segments. Percent correct was computed at each fragment density (8 levels), and individual subject data were fit with a logistic function, yielding slope (k) and point of subjective equality (PSE) parameters.

Trial-wise perceptual uncertainty was estimated by computing the entropy of the predicted probability of a correct response (p_c), derived from each subject's logistic fit. This produced an uncertainty measure that varied with stimulus density. These trial-level values were used in subsequent analyses.

Mixed-effects regression models were then fit to test how 1) accuracy and 2) confidence were predicted by density, uncertainty, and stimulus type. Models included random intercepts for subject (and object identity when available), and binomial link functions for accuracy (Table 1).

Table 4. Description of regression models constructed to examine the effects of decision-making variables and targets on behavioral responses

Model	Outcome Variable	Predictor Variables	Random Effects
Model 1 (binomial)	Accuracy	Fragment Type, Density, Uncertainty*, Fragment Type * Density, Fragment Type * Uncertainty, Reaction Time.	Participant, object ID
Model 2	Confidence	Fragment Type, Density, Uncertainty*, Fragment Type * Density, Accuracy, Reaction Time	Participant, object ID

Neuroimaging analysis

Neuroimaging analyis was performed using a mass univariate analysis in SPM12 (Wellcome Centre for Human Neuroimaging, UCL, UK www.fil.ion.ucl.ac.uk/spm). The generalized linear model was designed based on the behavioral models above, adapted for fMRI. The preprocessing pipeline applied to the functional MR datasets is described below.

Preprocessing

Functional MR volumes were first converted to niftii format from dicom. The two echo images for each volume of the fMRI time-series were combined using simple summation (Poser et al., 2006). Images were then slice-time corrected to the middle slice. Voxel displacement maps were computed from the B_0-field mapping data using SPM's Fieldmap

toolbox (Andersson et al., 2001) and inserted into the realign and unwarp step of SPM (6; 3 translational and 3 rotational). Individual T1w anatomical volumes were then co-registered to the mean functional images, followed by tissue classification and spatial registration to standard Montreal Neurological Institute (MNI) space using SPM12s "unified segmentation". The resulting parameters (forward deformations) were then applied to functional volumes, before applying a Gaussian 3D smoothing with 8mm full-width-at-half-maximum smoothing kernel. The resulting preprocessed images were used for statistical analysis.

Voxelwise analysis

We estimated subject-level event-related GLMs in SPM12. Each participant contributed two EPI runs (TR = 2.48 s) modeled separately within a single design matrix. Regressors were convolved with the canonical hemodynamic response function. Low-frequency drifts were attenuated with a 128 s high-pass filter and serial correlations were modeled using FAST. Analyses were restricted to voxels within SPM's intracranial volume mask; the implicit baseline served as the reference.

The first-level GLM included the following event onsets: (1) cue onsets corresponding to cue image presentation; (2) button-press responses; and (3) confidence reports. Each event type was modeled as a zero-duration (stick) function. Cue onsets were modeled separately for *phosphene* and *segment* fragment types, each parametrically modulated by (i) the fragment density value and (ii) its associated uncertainty, defined as the entropy value computed from behavioral data. RGB and contour trials were modeled as control conditions without modulators. Response events were modeled separately for phosphene and segment trials and were parametrically modulated by accuracy and reaction time. Confidence events were likewise modeled separately for the two fragment types and parametrically modulated by the confidence rating and reaction time. Within each condition, serial orthogonalization of parametric modulators was retained, such that variance was first attributed to the earlier modulator before the subsequent one.

Nuisance predictors included the six rigid-body head-motion parameters and 18 physiological regressors derived using RETROICOR (via the TAPAS PhysIO toolbox; Frässle et al., 2021) to capture respiration, cardiac phase, and interaction terms.

Model estimation used SPM's "Classical" ordinary least squares. The mass univariate analyses tested effects associated with (i) phosphene trial onsets, (ii) segment trial onsets, and (iii) their direct contrasts, as well as the corresponding parametric effects of density, accuracy, and confidence. Additional contrasts pooled across fragment types to examine main effects of correct responses, density, and confidence, and compared fragmented-image trials with contour and RGB control trials. Statistical inference at the group level used a cluster-forming threshold of voxel-wise $p < 0.001$ (uncorrected, $k = 25$) and a family-wise error (FWE) correction at $p < 0.05$, following current best-practice recommendations (*Eklund et al.*, 2016).

ROI analysis

Because the research question focuses on visual areas involved in object recognition, four *a priori* regions of interest (ROIs) were selected for region.based analysis: V1, V4, and the lateral occipital complex (LOC) in the visual cortex (L. Wang et al., 2015), in addition to the anterior cingulate cortex. Within each ROI, results were considered significant at $p < 0.05$, voxel-level FWE corrected using small-volume correction (Figure 4b).

Mediation Analysis

To determine which brain regions mediate the relationship between the empirically derived uncertainty of a stimulus at a given fragment type and density level and correct object recognition. Mediation was conducted in Matlab using the CanLab mediation toolbox (with a bootstrapping procedure (5000 samples) within a mask confined to regions of interest in the visual cortex (V1, V4 and LOC) and the anterior cingulate cortex,

Single-trial cue responses for mediation were estimated with a beta-series (LS-A) GLM in SPM12. For each run, we modeled every cue onset as a separate stick regressor (64 trials/run; 0-s duration), together with shared regressors for response onsets (parametric modulators: accuracy, RT), confidence reports (parametric modulators: rating, RT), and control cue types (RGB, contours). Nuisance regressors comprised 6 rigid-body motion parameters and 18 physiological terms (RETROICOR), and a 128-s high-pass filter was applied; serial correlations were modeled with FAST. This yielded 128 cue betas per subject (64 per run).

Mediation analysis used Canlab's multilevel brain mediation toolbox on *a priori* ROIs (mask comprising ACC, V1, V4, and LOC). The *X* variable was trial-wise perceptual uncertainty (Shannon entropy from each participant's psychometric function); the *Y* variable was trial-

wise accuracy (0/1); the mediator *M* was the vector of single-trial cue betas for each subject within the mask. Models were fit with random subject intercepts and bias-corrected bootstrap for inference (5000 samples); family-wise error within the mask was controlled by FDR and thresholding at q <0.05 on the voxelwise *p*-maps for the indirect path (*ab*). Fragment-type–specific models were obtained by gating *X* to phosphene or segment trials, with the same *M* and *Y*. Density was included as a covariate in all models.

Acknowledgments

We thank Jenny Schroeder for her instrumental contribution in neuroimaging data acquisition. We thank Prof. Udo Ernst and Dr. David Rotermund for providing the experimental stimuli used in the study.

CRediT

LLK: **Conceptualization ; Project Administration; Investigation; Methodology; Formal Analysis; Writing – Original Draft Preparation;**

ES: **Conceptualization ; Writing – Review & Editing**

AL: **Methodology; Investigation; Writing – Review & Editing**

MH: **Writing – Review & Editing; Supervision; Funding Acquisition**

BD: **Writing – Review & Editing; Supervision; Funding Acquisition**

References

Alexander, W. H., & Brown, J. W. (2014). *A general role for medial prefrontal cortex in event prediction*. *8*(July), 1–11. https://doi.org/10.3389/fncom.2014.00069

Andersson, J. L. R., Hutton, C., Ashburner, J., Turner, R., & Friston, K. (2001). Modeling Geometric Deformations in EPI Time Series. *NeuroImage*, *13*(5), 903–919. https://doi.org/10.1006/nimg.2001.0746

Balsdon, T., Mamassian, P., & Wyart, V. (2021). Separable neural signatures of confidence during perceptual decisions. *eLife*, *10*, e68491. https://doi.org/10.7554/eLife.68491

Biederman, I. (1987). Recognition-by-components: A theory of human image understanding. *Psychological Review*, *94*(2), 115–147. https://doi.org/10.1037/0033-295X.94.2.115

Borda, E., & Ghezzi, D. (2022). Advances in visual prostheses: Engineering and biological challenges. *Progress in Biomedical Engineering*, *4*(3), 032003. https://doi.org/10.1088/2516-1091/ac812c

Bosking, W. H., Oswalt, D. N., Foster, B. L., Sun, P., Beauchamp, M. S., & Yoshor, D. (2022). Percepts evoked by multi-electrode stimulation of human visual cortex. *Brain Stimulation*, *15*(5), 1163–1177. https://doi.org/10.1016/j.brs.2022.08.007

Brodeur, M. B., Dionne-Dostie, E., Montreuil, T., & Lepage, M. (2010). The Bank of Standardized Stimuli (BOSS), a New Set of 480 Normative Photos of Objects to Be Used as Visual Stimuli in Cognitive Research. *PLOS ONE*, *5*(5), e10773. https://doi.org/10.1371/journal.pone.0010773

Carlson, E. T., Rasquinha, R. J., Zhang, K., & Connor, C. E. (2011). A Sparse Object Coding Scheme in Area V4. *Current Biology*, *21*(4), 288–293. https://doi.org/10.1016/j.cub.2011.01.013

Chen, S. C., Suaning, G. J., Morley, J. W., & Lovell, N. H. (2009). Simulating prosthetic vision: I. Visual models of phosphenes. *Vision Research*, *49*(12), 1493–1506. https://doi.org/10.1016/j.visres.2009.02.003

Chen, S., Weidner, R., Zeng, H., Fink, G. R., Müller, H. J., & Conci, M. (2021). Feedback from lateral occipital cortex to V1/V2 triggers object completion: Evidence from functional magnetic resonance imaging and dynamic causal modeling. *Human Brain Mapping*, *42*(17), 5581–5594. https://doi.org/10.1002/hbm.25637

Choi, H., Pasupathy, A., & Shea-Brown, E. (2018). Predictive Coding in Area V4: Dynamic Shape Discrimination under Partial Occlusion. *Neural Computation*, *30*(5), 1209–1257. https://doi.org/10.1162/NECO_a_01072

Dagnino, B., Gariel-Mathis, M.-A., & Roelfsema, P. R. (2015). Microstimulation of area V4 has little effect on spatial attention and on perception of phosphenes evoked in area

V1. *Journal of Neurophysiology*, *113*(3), 730–739. https://doi.org/10.1152/jn.00645.2014

Erickson-Davis, C., & Korzybska, H. (2021). What do blind people "see" with retinal prostheses? Observations and qualitative reports of epiretinal implant users. *PLOS ONE*, *16*(2), e0229189. https://doi.org/10.1371/journal.pone.0229189

Fernández, E., Alfaro, A., Soto-Sánchez, C., Gonzalez-Lopez, P., Lozano, A. M., Peña, S., Grima, M. D., Rodil, A., Gómez, B., Chen, X., Roelfsema, P. R., Rolston, J. D., Davis, T. S., & Normann, R. A. (2021). Visual percepts evoked with an intracortical 96-channel microelectrode array inserted in human occipital cortex. *The Journal of Clinical Investigation*, *131*(23), e151331. https://doi.org/10.1172/JCI151331

Fine, I., & Boynton, G. M. (2024). A virtual patient simulation modeling the neural and perceptual effects of human visual cortical stimulation, from pulse trains to percepts. *Scientific Reports*, *14*(1), 17400. https://doi.org/10.1038/s41598-024-65337-1

Frässle, S., Aponte, E. A., Bollmann, S., Brodersen, K. H., Do, C. T., Harrison, O. K., Harrison, S. J., Heinzle, J., Iglesias, S., Kasper, L., Lomakina, E. I., Mathys, C., Müller-Schrader, M., Pereira, I., Petzschner, F. H., Raman, S., Schöbi, D., Toussaint, B., Weber, L. A., … Stephan, K. E. (2021). TAPAS: An Open-Source Software Package for Translational Neuromodeling and Computational Psychiatry. *Frontiers in Psychiatry*, *12*. https://doi.org/10.3389/fpsyt.2021.680811

Gold, J. I., & Stocker, A. A. (2017). Visual Decision-Making in an Uncertain and Dynamic World. *Annual Review of Vision Science*, *3*(Volume 3, 2017), 227–250. https://doi.org/10.1146/annurev-vision-111815-114511

Granley, J., Fauvel, T., Chalk, M., & Beyeler, M. (2023). Human-in-the-Loop Optimization for Deep Stimulus Encoding in Visual Prostheses. *Advances in Neural Information Processing Systems*, *36*, 79376–79398.

Kéri, S., Decety, J., Roland, P. E., & Gulyás, B. (2004). Feature uncertainty activates anterior cingulate cortex. *Human Brain Mapping*, *21*(1), 26–33. https://doi.org/10.1002/hbm.10150

Kienitz, R., Kouroupaki, K., & Schmid, M. C. (2022). Microstimulation of visual area V4 improves visual stimulus detection. *Cell Reports*, *40*(12), 111392. https://doi.org/10.1016/j.celrep.2022.111392

Kiral-Kornek, F. I., O'Sullivan-Greene, E., Savage, C. O., McCarthy, C., Grayden, D. B., & Burkitt, A. N. (2014). Improved visual performance in letter perception through edge orientation encoding in a retinal prosthesis simulation. *Journal of Neural Engineering*, *11*(6), 066002. https://doi.org/10.1088/1741-2560/11/6/066002

Kuai, S.-G., Li, W., Yu, C., & Kourtzi, Z. (2017). Contour Integration over Time: Psychophysical and fMRI Evidence. *Cerebral Cortex (New York, N.Y.: 1991)*, *27*(5), 3042–3051. https://doi.org/10.1093/cercor/bhw147

Lawrence, S. J. D., Zamboni, E., Vernon, R. J. W., Gouws, A. D., Wade, A. R., & Morland, A. B. (2023). The Emergence of Tuning to Global Shape Properties of Radial Frequency Patterns in the Ventral Visual Pathway. *The Journal of Neuroscience: The Official Journal of the Society for Neuroscience*, *43*(29), 5378–5390. https://doi.org/10.1523/JNEUROSCI.2237-22.2023

Levinson, M., Podvalny, E., Baete, S. H., & He, B. J. (2021). Cortical and subcortical signatures of conscious object recognition. *Nature Communications*, *12*(1), 2930. https://doi.org/10.1038/s41467-021-23266-x

Liu, X., Chen, P., Ding, X., Liu, A., Li, P., Sun, C., & Guan, H. (2022). A narrative review of cortical visual prosthesis systems: The latest progress and significance of nanotechnology for the future. *Annals of Translational Medicine*, *10*(12), 716. https://doi.org/10.21037/atm-22-2858

Lonnqvist, B., Scialom, E., Gokce, A., Merchant, Z., Herzog, M. H., & Schrimpf, M. (2025). *Contour Integration Underlies Human-Like Vision* (arXiv:2504.05253). arXiv. https://doi.org/10.48550/arXiv.2504.05253

Meuwese, J. D. I., van Loon, A. M., Lamme, V. A. F., & Fahrenfort, J. J. (2014). The subjective experience of object recognition: Comparing metacognition for object detection and object categorization. *Attention, Perception, & Psychophysics*, *76*(4), 1057–1068. https://doi.org/10.3758/s13414-014-0643-1

Michel, M., Gao, Y., Mazor, M., Kletenik, I., & Rahnev, D. (2024). When visual metacognition fails: Widespread anosognosia for visual deficits. *Trends in Cognitive Sciences*, *28*(12), 1066–1077. https://doi.org/10.1016/j.tics.2024.09.003

Mineault, P. J., Zanos, T. P., & Pack, C. C. (2013). Local field potentials reflect multiple spatial scales in V4. *Frontiers in Computational Neuroscience*, *7*. https://doi.org/10.3389/fncom.2013.00021

Molenberghs, P., Trautwein, F.-M., Böckler, A., Singer, T., & Kanske, P. (2016). Neural correlates of metacognitive ability and of feeling confident: A large-scale fMRI study. *Social Cognitive and Affective Neuroscience*, *11*(12), 1942–1951. https://doi.org/10.1093/scan/nsw093

O'Reilly, J. X., Schuffelgen, U., Cuell, S. F., Behrens, T. E. J., Mars, R. B., & Rushworth, M. F. S. (2013). Dissociable effects of surprise and model update in parietal and anterior cingulate cortex. *Proceedings of the National Academy of Sciences*, *110*(38), E3660–E3669. https://doi.org/10.1073/pnas.1305373110

Oswalt, D., Bosking, W., Sun, P., Sheth, S. A., Niketeghad, S., Salas, M. A., Patel, U., Greenberg, R., Dorn, J., Pouratian, N., Beauchamp, M., & Yoshor, D. (2021). Multi-electrode stimulation evokes consistent spatial patterns of phosphenes and improves

phosphene mapping in blind subjects. *Brain Stimulation*, *14*(5), 1356–1372. https://doi.org/10.1016/j.brs.2021.08.024

Parvizi, J., Jacques, C., Foster, B. L., Witthoft, N., Rangarajan, V., Weiner, K. S., & Grill-Spector, K. (2012). Electrical stimulation of human fusiform face-selective regions distorts face perception. *The Journal of Neuroscience: The Official Journal of the Society for Neuroscience*, *32*(43), 14915–14920. https://doi.org/10.1523/JNEUROSCI.2609-12.2012

Pasupathy, A., Popovkina, D. V., & Kim, T. (2020). Visual Functions of Primate Area V4. *Annual Review of Vision Science*, *6*, 363–385. https://doi.org/10.1146/annurev-vision-030320-041306

Phylactou, P., Traikapi, A., & Konstantinou, N. (2023). One in four people fail to perceive phosphenes during early visual cortex transcranial magnetic stimulation. *Brain Stimulation: Basic, Translational, and Clinical Research in Neuromodulation*, *16*(1), 23–24. https://doi.org/10.1016/j.brs.2022.12.012

Poser, B. A., Versluis, M. J., Hoogduin, J. M., & Norris, D. G. (2006). BOLD contrast sensitivity enhancement and artifact reduction with multiecho EPI: Parallel-acquired inhomogeneity-desensitized fMRI. *Magnetic Resonance in Medicine*, *55*(6), 1227–1235. https://doi.org/10.1002/mrm.20900

Rangarajan, V., Hermes, D., Foster, B. L., Weiner, K. S., Jacques, C., Grill-Spector, K., & Parvizi, J. (2014). Electrical stimulation of the left and right human fusiform gyrus causes different effects in conscious face perception. *The Journal of Neuroscience: The Official Journal of the Society for Neuroscience*, *34*(38), 12828–12836. https://doi.org/10.1523/JNEUROSCI.0527-14.2014

Roe, A. W., Chelazzi, L., Connor, C. E., Conway, B. R., Fujita, I., Gallant, J. L., Lu, H., & Vanduffel, W. (2012). Toward a Unified Theory of Visual Area V4. *Neuron*, *74*(1), 12–29. https://doi.org/10.1016/j.neuron.2012.03.011

Rushworth, M. F. S., & Behrens, T. E. J. (2008). Choice, uncertainty and value in prefrontal and cingulate cortex. *Nature Neuroscience*, *11*(4), 389–397. https://doi.org/10.1038/nn2066

Sanchez-Garcia, M., Martinez-Cantin, R., & Guerrero, J. J. (2018). *Structural and object detection for phosphene images* (arXiv:1809.09607). arXiv. https://doi.org/10.48550/arXiv.1809.09607

Schaeffner, L. F., & Welchman, A. E. (2017). Mapping the visual brain areas susceptible to phosphene induction through brain stimulation. *Experimental Brain Research*, *235*(1), 205–217. https://doi.org/10.1007/s00221-016-4784-4

Scialom, E., Ernst, U. A., Rotermund, D., & Herzog, M. H. (2024). *Minimizing the number of phosphenes required for object recognition under prosthetic vision* (p. 2024.09.26.614440). bioRxiv. https://doi.org/10.1101/2024.09.26.614440

Shiozaki, H. M., Tanabe, S., Doi, T., & Fujita, I. (2012). Neural Activity in Cortical Area V4 Underlies Fine Disparity Discrimination. *Journal of Neuroscience*, *32*(11), 3830–3841. https://doi.org/10.1523/JNEUROSCI.5083-11.2012

Torfs, K., Panis, S., & Wagemans, J. (2010). Identification of fragmented object outlines: A dynamic interplay between different component processes. *Visual Cognition*, *18*(8), 1133–1164. https://doi.org/10.1080/13506281003693593

van der Grinten, M., de Ruyter van Steveninck, J., Lozano, A., Pijnacker, L., Rueckauer, B., Roelfsema, P., van Gerven, M., van Wezel, R., Güçlü, U., & Güçlütürk, Y. (2024). Towards biologically plausible phosphene simulation for the differentiable

optimization of visual cortical prostheses. *eLife*, *13*, e85812. https://doi.org/10.7554/eLife.85812

Wang, L., Mruczek, R. E. B., Arcaro, M. J., & Kastner, S. (2015). Probabilistic Maps of Visual Topography in Human Cortex. *Cerebral Cortex (New York, N.Y.: 1991)*, *25*(10), 3911–3931. https://doi.org/10.1093/cercor/bhu277

Wang, Y., Ma, N., He, X., Li, N., Wei, Z., Yang, L., Zha, R., Han, L., Li, X., Zhang, D., Liu, Y., & Zhang, X. (2017). Neural substrates of updating the prediction through prediction error during decision making. *NeuroImage*, *157*, 1–12. https://doi.org/10.1016/j.neuroimage.2017.05.041

Wei, H., Dong, Z., & Wang, L. (2018). V4 shape features for contour representation and object detection. *Neural Networks*, *97*, 46–61. https://doi.org/10.1016/j.neunet.2017.09.010

Winawer, J., & Witthoft, N. (2015). Human V4 and ventral occipital retinotopic maps. *Visual Neuroscience*, *32*, E020. https://doi.org/10.1017/S0952523815000176

Wyatte, D., Jilk, D. J., & O'Reilly, R. C. (2014). Early recurrent feedback facilitates visual object recognition under challenging conditions. *Frontiers in Psychology*, *5*. https://doi.org/10.3389/fpsyg.2014.00674

Zamboni, E., Watson, I., Stirnberg, R., Huber, L., Formisano, E., Goebel, R., Kennerley, A. J., & Morland, A. B. (2025). Mapping curvature domains in human V4 using CBV-sensitive layer-fMRI at 3T. *Frontiers in Neuroscience*, *19*. https://doi.org/10.3389/fnins.2025.1537026

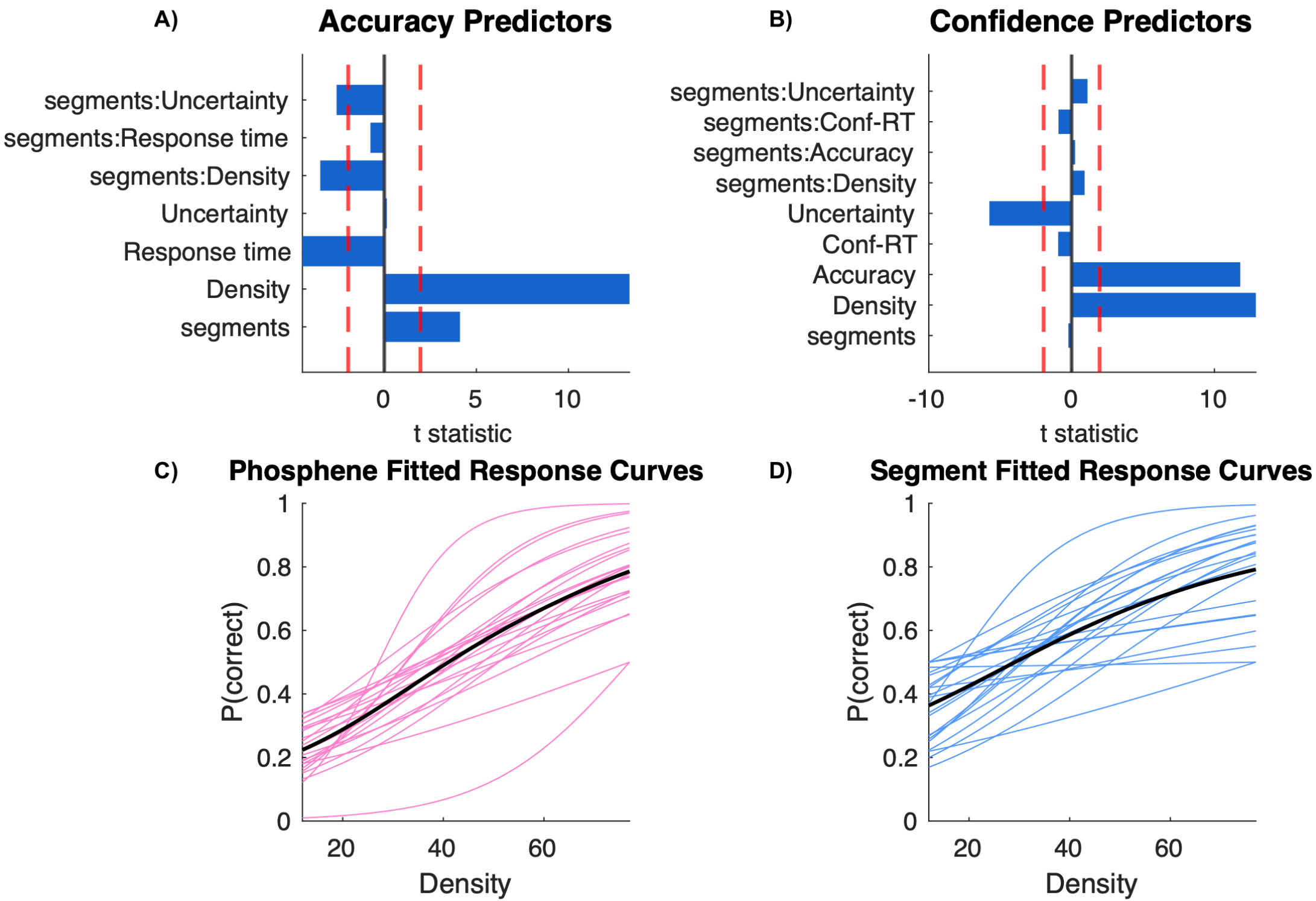
A)
Accuracy Predictors
segments:Uncertainty
segments:Response time
segments:Density
Uncertainty
Response time
Density
segments
0
5
10
t statistic
B)
Confidence Predictors
segments:Uncertainty
segments:Conf-RT
segments:Accuracy
segments:Density
Uncertainty
Conf-RT
Accuracy
Density
segments
-10
0
10
t statistic
C)
Phosphene Fitted Response Curves
P(correct)
1
0.8
0.6
0.4
0.2
0
20
40
60
Density
D)
Segment Fitted Response Curves
P(correct)
1
0.8
0.6
0.4
0.2
0
20
40
60
Density

Whole-Brain Main Effects and Parametrics

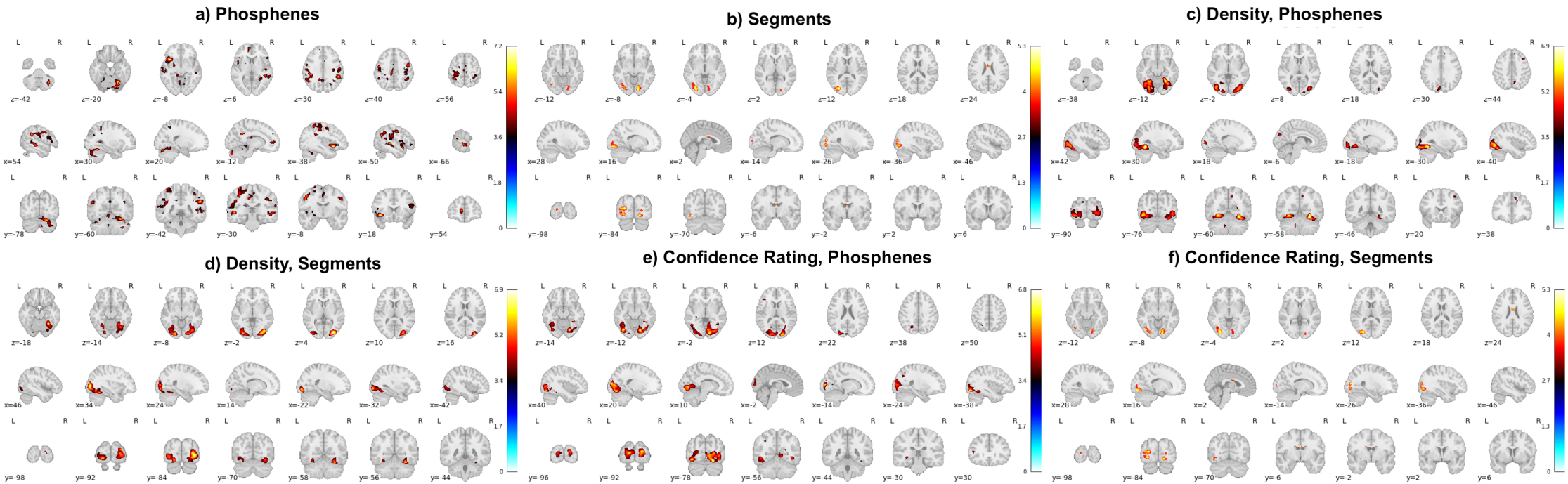

a) Contrast map, for correct segment vs phosphene trial responses

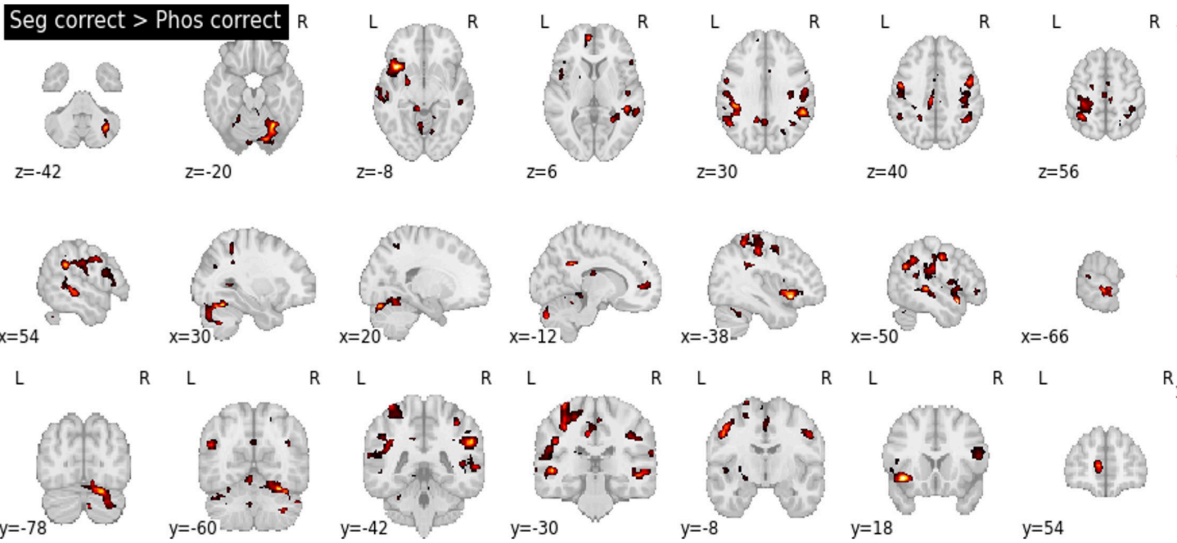

b) Overlap of correct segment vs phosphene trials (orange) and V4 (blue)

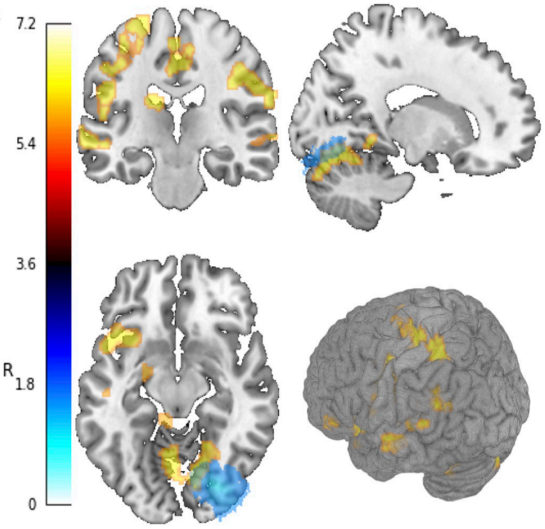

c) ACC mediating cluster between stimulus uncertainty and accurate phophene trials

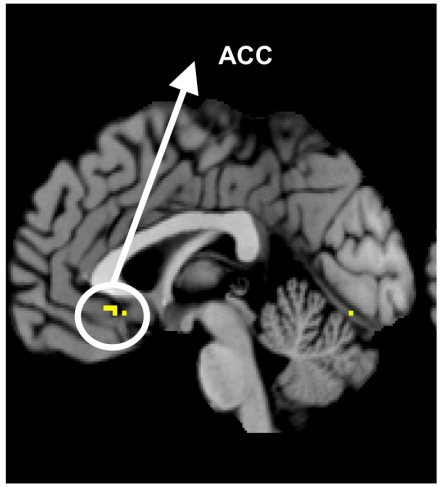

a) Sample Trial

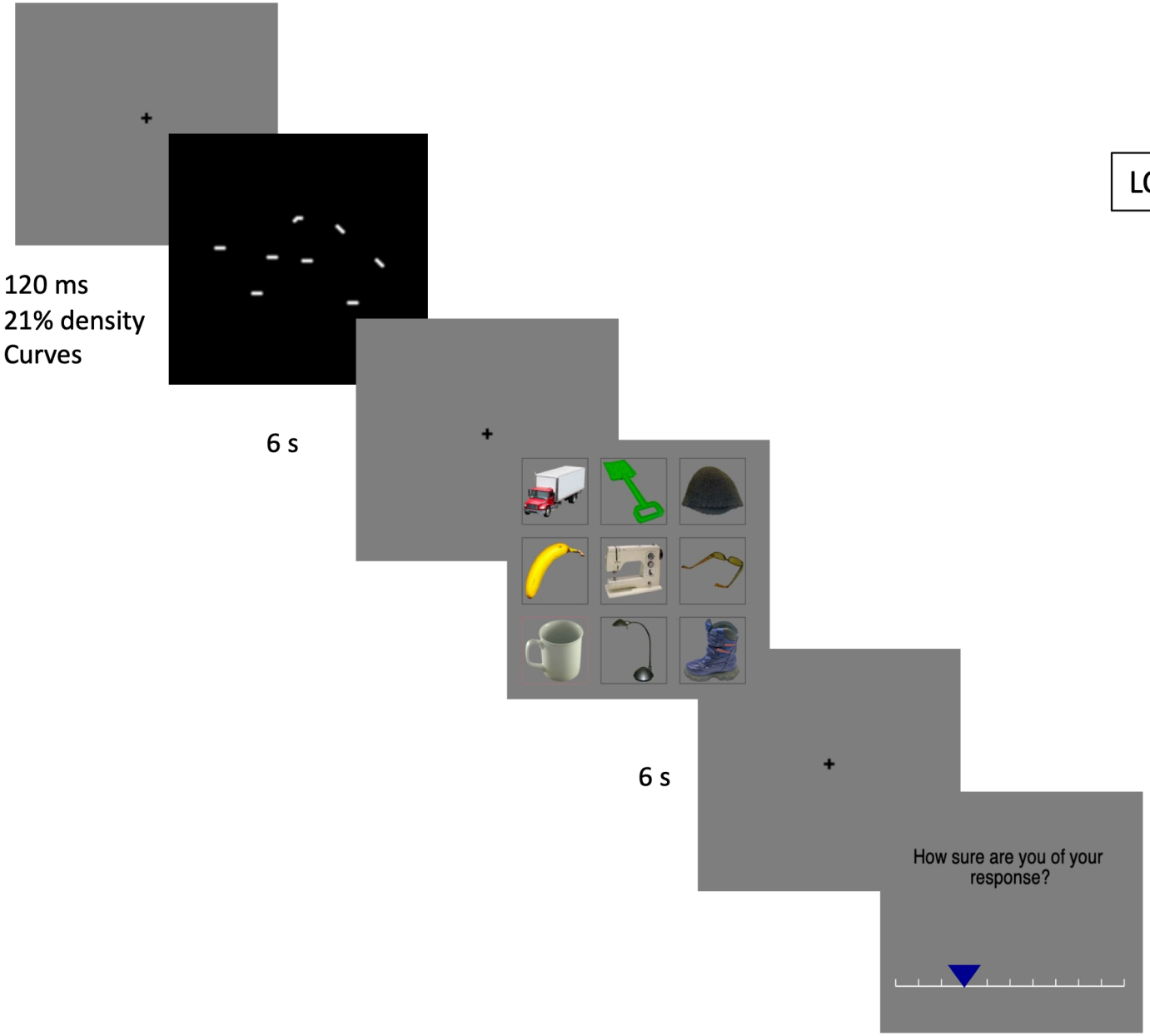
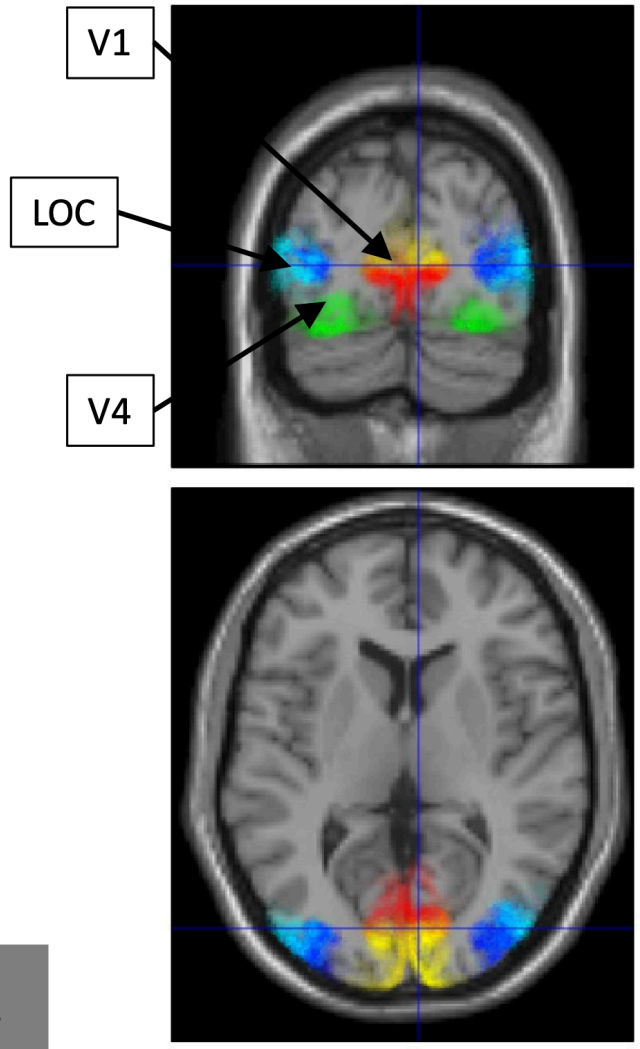
b) Retinotopic Atlas for V1, V4 and Lateral Occipital Cortex